On the $\tilde{A}$ and $\tilde{B}$ electronic states of NCO and its clusters with nonpolar solvents

Jianlong Yao, Jose A. Fernandez, and Elliot R. Bernstein

Citation: The Journal of Chemical Physics **107**, 8813 (1997); doi: 10.1063/1.475173
View online: http://dx.doi.org/10.1063/1.475173
View Table of Contents: http://aip.scitation.org/toc/jcp/107/21
Published by the American Institute of Physics

On the $\tilde{A}$ and $\tilde{B}$ electronic states of NCO and its clusters with nonpolar solvents

Jianlong Yao, Jose A. Fernandez, and Elliot R. Bernstein
Department of Chemistry, Colorado State University, Fort Collins, Colorado 80523-1872

(Received 18 June 1997; accepted 25 August 1997)

The $\tilde{B}\leftarrow\tilde{X}$ and $\tilde{A}\leftarrow\tilde{X}$ transitions of the NCO radical and its clusters with nonpolar solvents are studied in a supersonic jet expansion by employing laser-induced fluorescence techniques. Fluorescence excitation (FE) and hole burning spectra are recorded for the NCO radical and compared to previous work. NCO is clustered with Ar, N_2, CH_4, and CF_4 nonpolar molecules to elucidate the effect of solvation on the radical energy levels and dynamics. FE spectra are detected for NCO 1:1 clusters showing blue shifts in their spectra with respect to that of the isolated NCO radical, while their 1:n counterparts show either red or blue shifts. Potential energy surface calculations are performed to evaluate the binding energies and geometries of 1:1 clusters in the $\tilde{X}$, $\tilde{A}$, and $\tilde{B}$ electronic states. The relatively long decay lifetime and red shifted fluorescence wavelength range observed for $\tilde{B}$ state clusters suggests that they decay first through internal conversion (IC) to $\tilde{A}$ vibronic levels, and then experience rapid intracluster vibrational redistribution (IVR) and vibrational predissociation (VP), yielding ground state solvent molecules and NCO radicals at lower $\tilde{A}$ vibronic levels. These $\tilde{A}$ state NCO radicals subsequently emit, generating the $\tilde{A}\rightarrow\tilde{X}$ band. © *1997 American Institute of Physics.* [S0021-9606(97)00845-3]

I. INTRODUCTION

The study of the NCO radical has both practical and theoretical significance. NCO is involved in the combustion process of nitrogen-containing fuels[1–4] and the decomposition of nitrogen-containing organic compounds such as amines.[5] Most of the NCO studies fall into roughly the following categories: its formation,[1–9] kinetics,[10,11] rovibronic structure,[12–29] and predissociation.[12,19,21,22]

Similar to CO_2^+, BO_2, and N_3, NCO is a linear triatomic molecule with an open shell structure containing 15 electrons. The ground and first two excited states of NCO have electronic configurations $\ldots(1\pi)^4(\sigma)^2(2\pi)^3$, $\ldots(1\pi)^4(\sigma)^1(2\pi)^4$, and $\ldots(1\pi)^3(\sigma)^2(2\pi)^4$, respectively. The rovibronic structure of NCO is notoriously complicated: it arises from spin–orbital interactions, the Renner–Teller effect, Herzberg–Teller coupling, Fermi resonance, and other perturbations. Dixon and co-workers[12,13] studied the first two electronic transitions of NCO in some detail. Complementary work on the $\tilde{A}\leftarrow\tilde{X}$ transition includes a number of optical absorption[14,23] and fluorescence studies.[15–20] The ground state of NCO has also been subjected to a variety of spectroscopic studies.[23–29] One of the major focal points for many of these studies has been characterization of the Renner–Teller effect in the ground state rovibronic levels.

The $B\ ^2\Pi\leftarrow\tilde{X}\ ^2\Pi$ transition of NCO is much less well studied than the $\tilde{A}\ ^2\Sigma^+\leftarrow\tilde{X}$ transition due to apparent difficulties caused by Renner–Teller and Fermi resonance interactions within the $\tilde{B}\ ^2\Pi$ state, and strong coupling between the $\tilde{B}\ ^2\Pi$ and $\tilde{A}\ ^2\Sigma^+$ vibronic levels. Dixon *et al.*[13] obtained a rotational analysis of the $\tilde{B}\ ^2\Pi_i(000)$ state of NCO by using an optical–optical double resonance (OODR) technique. Recent interest has been drawn to the photodissociation of the NCO radical excited to its $\tilde{A}$ and $\tilde{B}$ state vibronic levels with comparable energy.

Alexander and Werner[30] carried out extensive calculations on the electronic structures of the NCO radical. They find a crossing between the $\tilde{A}$ and $\tilde{B}$ potential surfaces, and another crossing between the $\tilde{A}$ state and a repulsive $^4\Sigma^-$ state that correlates with the ground state asymptote $N(^4S)+CO(^1\Sigma^+)$, as indicated in a schematic diagram in Fig. 1. The crossing between the $\tilde{A}$ and $\tilde{B}$ states lies only a few hundreds wave numbers above the $\tilde{B}$ state energy minimum, and the other crossing is only slightly lower in energy. These crossings suggest that $\tilde{B}$ state vibronic levels with an energy lower than the $[N(^2D)+CO(^1\Sigma^+)]$ energy [near $\tilde{B}(600)$] can dissociate through two different surface crossings. The fast ion beam experiment done by Neumark's group[22] demonstrates that all vibronic levels of the $\tilde{B}$ state are dissociative. They confirm that the first few vibronic levels of the NCO B state indeed undergo spin-forbidden dissociation to $N(^4S)+CO(^1\Sigma^+)$, while the higher levels are dominated by the spin-allowed dissociation $N(^2D)+CO(^1\Sigma^+)$. Dagdigian's group[21] has determined the lifetimes of many $\tilde{A}$ state vibronic levels as well as some $\tilde{B}$ state vibronic levels in the wave number range of 27 300–32 900 cm^{-1}, and found that the onset of predissociation occurs at energies even slightly lower than the $\tilde{B}(000)$ level.

In this paper, we present laser-induced fluorescence (LIF) experiments on NCO and its clusters with nonpolar solvents Ar, N_2, CH_4, and CF_4 cooled in a supersonic jet expansion. FE spectra, fluorescence lifetimes, and fluorescence wavelength ranges are recorded for the $\tilde{A}\leftrightarrow\tilde{X}$, and $\tilde{B}\leftrightarrow\tilde{X}$ transitions of NCO and its clusters in order to under-

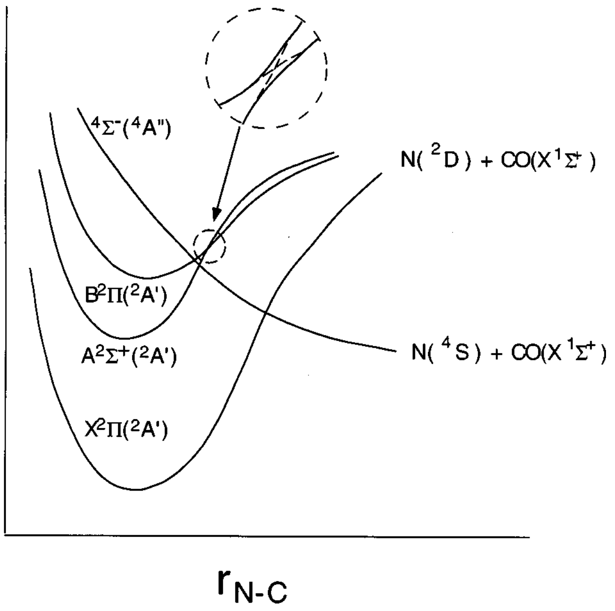

FIG. 1. $\tilde{A}$ schematic diagram of the electronic state potential curves of NCO, with fixed $r_{\text{C–O}}$ and θ_{NCO}. The labels A' and A'' are group representations for the C_S group of the nonlinear NCO radical ($\theta_{\text{NCO}}<180°$).

stand more about the vibronic structure of NCO, to study the geometry and binding energy of NCO clusters, and to compare the different fluorescence decay behavior of NCO and its clusters. The hole burning technique is used to verify vibronic transitions arising from the same ground state energy levels. Potential energy surface calculations and other computational techniques are employed to determine cluster geometry and binding energy in the $\tilde{X}$, $\tilde{A}$, and $\tilde{B}$ states of NCO.

II. PROCEDURES

A. Experiment

As is described in previous work,[31,32] the experiment is carried out in a stainless steel vacuum chamber at a pressure of *ca.* 10^{-4} Torr. In this work, liquid precursor phenylisocynate (Aldrich) contained in a glass boat is placed in the He backing gas line at room temperature. The precursor molecule is carried through a General Valve pulsed nozzle into a quartz tube ($0.7\,\text{mm}\ i.d.\times 10\,\text{mm}$) mounted at the exit of the nozzle. A 193 nm excimer laser with an energy of 80 mJ/pulse is focused into the quartz tube to photodissociate the precursor to form the NCO radical in high concentration. Radicals formed are rotationally cooled to roughly 10 K or even lower temperature upon the expansion at the exit of the quartz tube.

A second laser (Nd/YAG pumped dye laser) is used to excite the NCO radical roughly 2 cm downstream. Coumarin 440 dye laser fundamental output is used to excite the $\tilde{A}\leftarrow\tilde{X}$ transition of NCO, while the fundamental output of an R640 and DCM mixture is doubled to excite the $\tilde{B}\leftarrow\tilde{X}$ transition. The induced fluorescence is collected perpendicularly to the laser/molecular jet plane with a 5 cm focal length lens and detected with a C31034A RCA photomultiplier tube.

When performing cluster studies, the appropriate percentage of solvent is mixed into the helium carrier gas. Other procedures are the same as those reported for our CH_3O study.[32] Different colored filters are used to collect fluorescence in the wavelength ranges of interest.

B. Theory

A rather extensive series of calculations is performed in order to analyze the experimental results. Cluster geometry and binding energy are obtained employing an atom–atom potential energy calculation.[31,32] All molecules are considered as rigid entities in this calculation. The interaction energy is determined as a sum of various terms: short range repulsion, induction/dispersion, Coulomb, and hydrogen bonding. The atom–atom potential energy surface is given by[33]

$$E_B=\sum_{i=1}^{n}\sum_{j=1}^{m}\{[(A_{ij}/r_{ij}^{12}-C_{ij}/r_{ij}^{6})(1-\delta_{ij}^{\text{hb}})+(A_{ij}^{\text{hb}}/r_{ij}^{12} -C_{ij}^{\text{hb}}/r_{ij}^{10})\,\delta_{ij}^{\text{hb}}]+q_iq_j/Dr_{ij}\}=V_{\text{vdW}}+V_{\text{hb}}+V_{\text{C}}, \tag{1}$$

in which

$$A_{ij}=(1/2)C_{ij}r_{\text{min}}^{6}$$

and

$$C_{ij}=(3/2)\alpha_i\alpha_j e(h/2\pi m_e^{1/2})/[(\alpha_i/N_i)^{1/2}+(\alpha_j/N_j)^{1/2}], \tag{2}$$

r_{ij} is the distance between atoms i and j of different molecules, r_{min} is the sum of van der Waals radii and is different for each pair of atoms, δ_{ij} equals 1 for hydrogen bonding situations and 0 otherwise, q_i, q_j are atomic charges, D is the dielectric constant, N_i is the effective number of electrons for each type of atom, m_e is the mass of an electron, i is the polarizability of atom i, and r_i is the van der Waals radius of atom i.

All the parameters in Eqs. (1) and (2) are available for the ground state systems, except for the atomic charges. Ground state atomic charges are obtained through *ab initio* calculations using the GAUSSIAN 94 programs[34] and experimental geometry. Ground state geometries and binding energies of NCO clusters are calculated with these data.

Parameters needed for excited state NCO radical clusters are not available in the literature. The charge distribution and geometry of $\tilde{A}$ and $\tilde{B}$ state NCO are calculated using GAUSSIAN 94 at the CASSCF(9,8)/D95 level and are listed in Table I. The atomic polarizabilities and van der Waals radii needed in Eqs. (1) and (2) are not readily calculated from *ab initio* procedures. To solve this problem and obtain excited state geometries and binding energies for NCO clusters, we choose to adjust α_i and r_i to obtain a binding energy of one cluster in a particular excited state, so that the spectroscopic shift thus obtained matches exactly the experimental shift. We then use the adjusted α_i and r_i values to do the same calculation for all the other clusters in the same excited state.

TABLE I. *Ab initio* calculation results for NCO properties as a function of the electronic state.[a]

Property		X	A	B
C–N (Å)		1.2204	1.1899	1.2790
C–O (Å)		1.2645	1.2140	1.3600
Charge	N	−0.087	−0.202	−0.122
	C	0.243	0.441	0.355
	O	−0.156	−0.239	−0.233
E (hartree)		−167.188 36	−167.078 03	−167.046 25
$T_{e\text{calc.}}$ (cm^{-1})			24 186	31 153
$T_{0\text{exp}}$ (cm^{-1})			22 800	31 768

[a] Using GAUSSIAN 94 (Ref. 34) at the CASSCF(9,8)/D95 level.

Spectroscopic shifts calculated in this way are not always of good quantitative accuracy, but are usually qualitatively correct.

Cluster geometry thus obtained allows reasonable rotational contour simulation and van der Waals frequency calculation, which in return justify the qualitative correctness of an oversimplified fitting procedure. Rotational simulations are performed using a program developed for asymmetric rotors.[35]

III. RESULTS AND DISCUSSION

A. Fluorescence spectra of NCO

Supersonic jet fluorescence excitation (FE) spectra of NCO are recorded for both $\tilde{A}\leftarrow\tilde{X}$ and $\tilde{B}\leftarrow\tilde{X}$ transitions. The spectra are much simplified compared to those reported previously due to intensive cooling of the NCO radical in the jet expansion.

The FE spectrum of NCO $\tilde{A}\leftarrow\tilde{X}$ transition is shown in Fig. 2. The three strong features are assigned as the (000)←(000), (010)←(010), and (010)←(000) bands of the $\tilde{A}\ {}^2\Sigma^+\leftarrow\tilde{X}\ {}^2\Pi_{3/2}$ transition. No bands of the $\tilde{A}\ {}^2\Sigma^+\leftarrow\tilde{X}\ {}^2\Pi_{1/2}$ transition are observed.

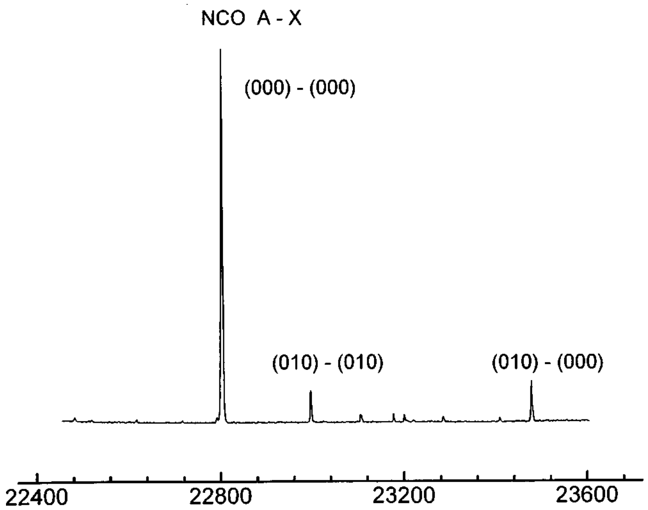

FIG. 2. FE spectrum of the NCO $\tilde{A}\ {}^2\Sigma^+\leftarrow\tilde{X}\ {}^2\Pi_{3/2}$ transition.

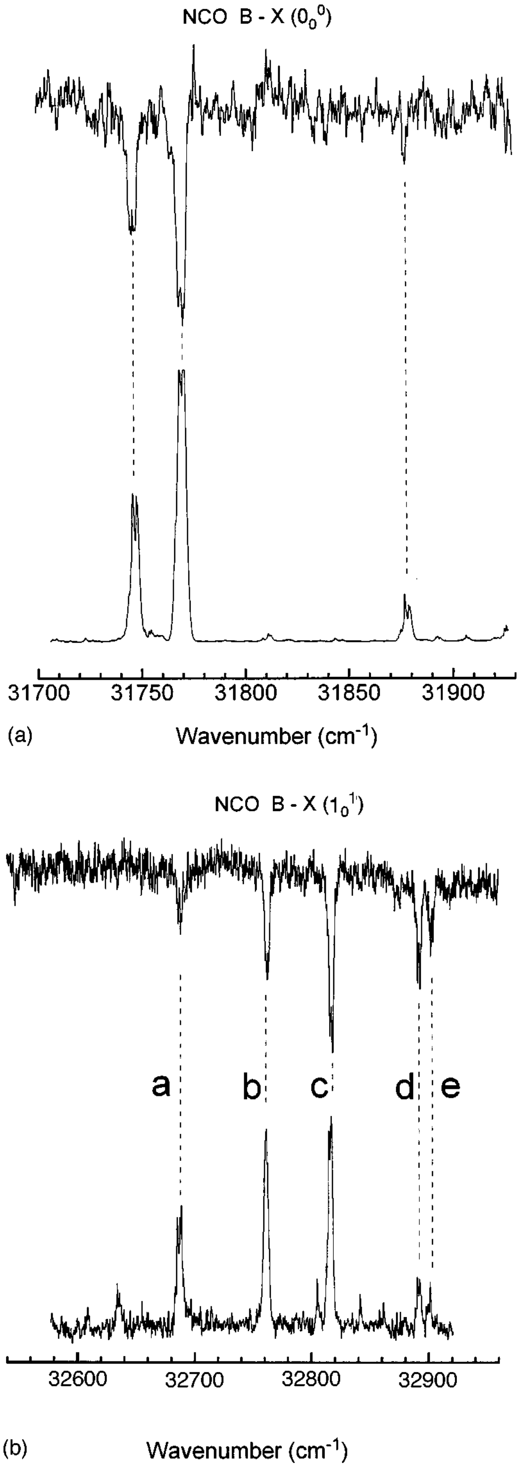

FIG. 3. (a) FE and hole burning spectra of NCO for the $\tilde{B}\ {}^2\Pi_{3/2}(000)\leftarrow\tilde{X}\ {}^2\Pi_{3/2}(000)$ transition region. The probe laser is set for $\tilde{A}\ {}^2\Sigma^+\leftarrow\tilde{X}\ {}^2\Pi_{3/2}$ at 22 800 cm^{-1}. (b) FE and hole burning spectra of NCO in the $\tilde{B}\ {}^2\Pi_{3/2}(100)\leftarrow\tilde{X}\ {}^2\Pi_{3/2}(000)$ transition region. The probe laser is set for the $\tilde{A}\ {}^2\Sigma^+\leftarrow\tilde{X}\ {}^2\Pi_{3/2}$ transition at 22 800 cm^{-1}.

Spectra of NCO $\tilde{B}\leftarrow\tilde{X}$ transition are more complicated due to the Renner–Teller effect, Fermi resonance, and the vibronic mixing between the $\tilde{A}$ and $\tilde{B}$ states. In Figs. 3(a) and 3(b) we present FE and hole burning spectra for the (000)←(000) and (100)←(000) band regions of the $\tilde{B}\ {}^2\Pi\leftarrow\tilde{X}\ {}^2\Pi$ transition. In the hole burning experiment, the probe laser is set at 22 800 cm^{-1}, the origin of the $\tilde{A}\ ^2\Sigma^+ \leftarrow \tilde{X}\ ^2\Pi_{3/2}$ transition. All the features appearing in hole burning spectra should arise from a common source, the $\tilde{X}\ ^2\Pi_{3/2}(000)$.

Vibronic structure in $\tilde{B}\ ^2\Pi(100) \leftarrow \tilde{X}\ ^2\Pi_{3/2}(000)$ transition region is reasonably well understood.[12,22] In Fig. 3(b), features b, c, and d at 32 761.4, 32 816.0, and 32 890.1 cm^{-1} can be assigned to μ-$\tilde{B}\ ^2\Pi_{3/2}(020) \leftarrow \tilde{X}\ ^2\Pi_{3/2}(000)$, $\tilde{B}\ ^2\Pi_{3/2}(100) \leftarrow \tilde{X}\ ^2\Pi_{3/2}(000)$, and κ-μ-$\tilde{B}\ ^2\Pi_{3/2}(020) \leftarrow \tilde{X}\ ^2\Pi_{3/2}(000)$ subbands, respectively, in agreement with Neumark *et al.*[22] The lifetimes of these $\tilde{B}\ ^2\Pi_{3/2}$ vibronic energy levels are all shorter than 10 ns, also in agreement with previous work.[19]

The feature at 32 690.0 cm^{-1} [a in Fig. 3(b)] is also observed by Neumark *et al.*[22] They suggest that it can be assigned as one of the two features of subband μ-$\tilde{B}\ ^2\Pi_{1/2}(020) \leftarrow \tilde{X}\ ^2\Pi_{1/2}(000)$, and that it results from extensive $\tilde{A}$ state perturbations. This is questionable since our hole burning spectrum indicates that this band also originates from $\tilde{X}\ ^2\Pi_{3/2}(000)$. Another weak feature e appears in both FE and hole burning spectra located at 32 901 cm^{-1}. This band can also be seen in the same spectrum by Neumark *et al.*, but they did not distinguish it from the 32 890 cm^{-1} band. Both features a and e may be $\tilde{A} \leftarrow \tilde{X}$ vibronic transitions arising from $\tilde{X}\ ^2\Pi_{3/2}(000)$ level.

The vibronic structure of the $\tilde{B}\ ^2\Pi_{3/2}(000) \leftarrow \tilde{X}\ ^2\Pi_{3/2}(000)$ region has been studied by Dixon *et al.*[13] and Dagdigian *et al.*[21] at high temperature. Dixon *et al.*[13] have extrapolated a $\tilde{B}\ ^2\Pi \leftarrow \tilde{X}\ ^2\Pi$ origin transition energy of 31 751 cm^{-1}. The vibronic bands of the same region obtained in our supersonic jet expansion appear somewhat different from those obtained at higher temperature.[13,21] As is shown in Fig. 3(a), hole burning indicates that the two strong features at 31 746.0 and 31 768.5 cm^{-1} share the same ground state level, $\tilde{X}\ ^2\Pi_{3/2}(000)$. These two strong bands cannot be simply $\tilde{A}$ vibronic bands since, within 650 cm^{-1} to the red of these two features, no other $\tilde{A}$ vibronic feature is found which has an intensity comparable to these. Most likely they arise from two transitions originating at $\tilde{X}\ ^2\Pi_{3/2}(000)$ and terminating at two vibronic levels that are generated by the mixing of $\tilde{B}\ ^2\Pi_{3/2}(000)$ with nearby $\tilde{A}$ vibronic levels. These features gain intensity mainly from the $B\ ^2\Pi_{3/2}(000)$ level.

The 31 768.5 cm^{-1} band in our spectrum appears to have more $\tilde{B}$ state character than the 31 746 cm^{-1} band. First, collecting all the fluorescence, the lifetimes of these excited states [near the (000) origin] are found to be 90 and 169 ns for 31 768.5 and 31 746.0 cm^{-1} bands, respectively. Second, as is shown in Fig. 4, by using different cut-off filters, the ratio of the 31 768.5 cm^{-1} band intensity to the 31 746.0 cm^{-1} band intensity decreases dramatically as the fluorescence collection wavelength range is red shifted to the $\tilde{A}$ state transition energy region. Dagdigian and co-workers[21] demonstrate that using a bandpass filter covering the $\tilde{A} \leftarrow \tilde{X}$ transition wavelength range, vibronic levels with more $\tilde{A}$ state character can be accentuated. Also in the same work, they demonstrate that vibronic levels with more $\tilde{B}$ character should have a shorter fluorescence lifetime, as is shown by a sharp dip in the decay lifetimes plot [Fig. 9 of Ref. 21(a)] in the vicinity of the $\tilde{B} \leftarrow \tilde{X}$ origin. Bearing this in mind, and considering our experimental result, the 31 768.5 cm^{-1} band has more $\tilde{B}\ ^2\Pi_{3/2}(000)$ character than does the one at 31 746.0 cm^{-1}.

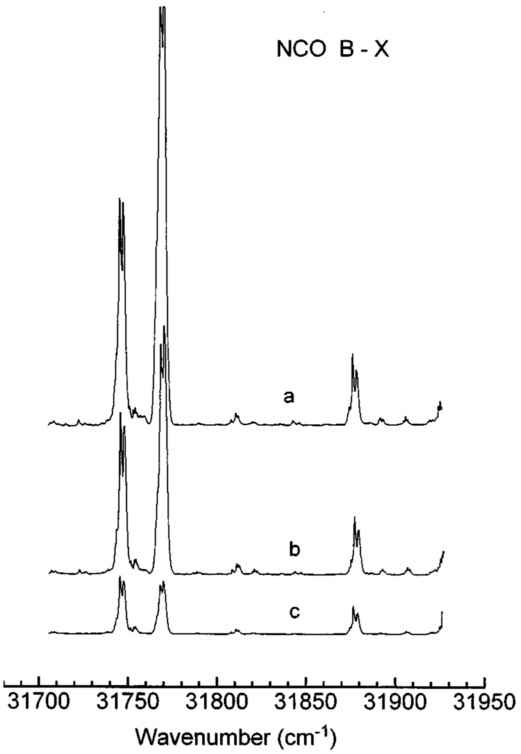

FIG. 4. The fluorescence signal collected for the NCO transition in the $\tilde{B}\ ^2\Pi_{3/2}(000) \leftarrow \tilde{X}\ ^2\Pi_{3/2}(000)$ region using (a) UV30, (b) L37, and (c) L42 colored filters in front of the PMT tube. The transmission ranges for these filters are to the red of 280, 350, and 410 nm, respectively.

Another band at 31 878.0 cm^{-1} has relatively high intensity with a lifetime comparable to that of the 31 746 cm^{-1} band. This feature may also be an $\tilde{A}$ state dominant vibronic band gaining intensity by mixing with the $\tilde{B}$ state 0^0 through vibronic coupling.

B. NCO clusters: Spectra and calculation

1. 1:1 clusters

Spectra–FE spectra are recorded for NCO clusters with one Ar, N_2, CH_4, or CF_4 molecule in both the NCO $\tilde{A} \leftarrow \tilde{X}$ and $\tilde{B} \leftarrow \tilde{X}$ transition regions. As is shown in Figs. 5(a) and 5(b), all cluster transition bands are located to the blue of corresponding NCO radical bands. This indicates a lower stabilization energy in the excited states of clusters compared to that in the ground state.

The $\tilde{A} \leftarrow \tilde{X}$ transition bands of NCO$(N_2)_1$ and NCO$(CF_4)_1$ are presented in Fig. 5(a). The spectra of each cluster contains around five features. The first feature of the two cluster bands are blue shifted 22.6 and 37.4 cm^{-1} with

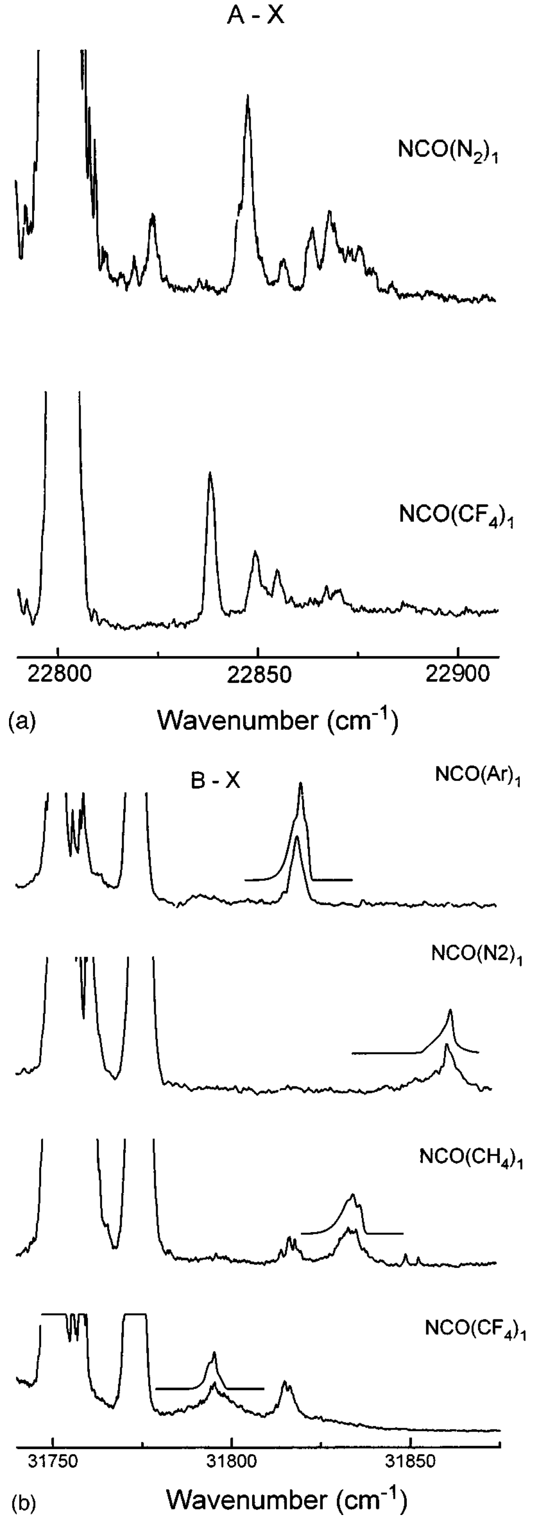

FIG. 5. (a) FE spectra of the $\tilde{A}\leftarrow\tilde{X}$ transition of NCO clustered with N_2 and CF_4. (b) FE spectra of the $\tilde{B}\leftarrow\tilde{X}$ transition of 1:1 NCO clusters. Simulated rotational envelopes are also shown for all cluster origin spectra.

respect to the NCO $\tilde{A}\leftarrow\tilde{X}$ origin at 22 800 cm^{-1}, respectively. Although backing pressure can be increased to as high as 500 psi, with either pure Ar or 30% CH_4 in He, we are not able to observe any features that can be assigned to the $\tilde{A}\leftarrow\tilde{X}$ transition of either NCO(Ar)$_1$ or NCO(CH$_4$)$_1$.

In the NCO $\tilde{B}\leftarrow\tilde{X}$ transition origin region, single features are observed for all the four clusters, as shown in Fig. 5(b). We assign this single feature in each cluster as arising from the 31 768.5 cm^{-1} bare radical feature for two reasons: (1) clustering with a nonpolar solvent like Ar, N_2, CH_4, and CF_4 should not remove the vibronic coupling between the $\tilde{A}$ and $\tilde{B}$ electronic states; and (2) cluster formation will certainly change the system dynamics and greatly shorten the lifetimes of the $\tilde{A}$ dominant vibronically coupled levels and in general not perturb the $\tilde{B}$ dominant level lifetime as much. Thus, the $\tilde{B}$ dominant feature should survive in the cluster spectra, while the $\tilde{A}$ dominant feature should not. Cluster dynamics in this energy range are discussed further below. The spectroscopic shifts of these cluster bands are thus 45.7, 58.5, 88.0, and 21.4 cm^{-1} for NCO clusters with Ar, CH_4, N_2, and CF_4, respectively. An interesting phenomenon observed for the $\tilde{B}\leftarrow\tilde{X}$ transition of these NCO clusters is that their fluorescence can only be detected to the red of 390 nm, and all features show a decay lifetime within the range of 250–320 ns, which is much longer than that of the $\tilde{B}$ state bare NCO radical. This will be discussed separately below.

Calculations—To extract information about the geometries and binding energies of these clusters in different electronic states, potential energy calculations are performed. Parameters that are needed for these calculations are listed in Tables I and II.

We first calculate all the binding energies and geometries of ground state clusters. The binding energies are listed in Table III, and the ground state geometries of the clusters are shown in Fig. 6. All the ground state clusters have only one minimum energy geometry with a solvent molecule attached to the side of the C═O bond in NCO.

For the $\tilde{B}$ state cluster potential energy surface, we adjust the α_i and r_{ii} values of the atoms in NCO to calculate the NCO(Ar)$_1$ binding energy, so that the calculated spectroscopic shift (i.e., the difference between this $\tilde{B}$ state binding energy and the ground state binding energy) matches exactly the experimental shift for the $\tilde{B}\leftarrow\tilde{X}$ transition. Then using the adjusted α_i and r_{ii} values, we calculate the binding energy for the other clusters in the $\tilde{B}$ state. As is listed in Table III, the spectroscopic shift thus calculated for the $\tilde{B}\leftarrow\tilde{X}$ transition of NCO(CH$_4$)$_1$ agrees very well with the experimental value. The calculated shift for NCO(N$_2$)$_1$ is 35% off the experimental shift, although two point charges are introduced (see Table II) to simulate the quadrupole moment of N_2. The calculated shift for NCO(CF$_4$)$_1$ is 110.3 cm^{-1} compared to the experimental value of 21.4 cm^{-1}. This rather poor agreement for NCO/CF$_4$ and N_2 clusters may be due to vibronic coupling between the $\tilde{A}$ and $\tilde{B}$ states and its changes for different clusters.

The calculated geometries for these 1:1 clusters in the $\tilde{B}$ electronic state are similar to those for the ground state.

Similar potential energy calculations are performed for the $\tilde{A}$ state clusters NCO(N$_2$)$_1$ and NCO(CF$_4$)$_1$ in the $\tilde{A}$ electronic state. Since the $\tilde{A}\leftarrow\tilde{X}$ transitions of NCO(Ar)$_1$ and NCO(CH$_4$)$_1$ are not observed, we sacrifice the NCO(N$_2$)$_1$

TABLE II. Parameters used for the cluster potential energy calculations.

		Charge			α_i (10^{-24} cm^3)			r_{ii} (A)[a]		
Molecule	Atom	X	A	B	X	A	B	X	A	B
	N	−0.087	−0.202	−0.122	0.93	1.26	0.98	3.51	3.93	4.22
NCO[b]	C	0.243	0.441	0.355	1.51	1.06	1.10	3.74	3.50	3.70
	O	−0.156	−0.239	−0.233	0.84	0.93	0.89	3.12	3.58	3.72
CF_4[c]	C	0.984			1.51			3.74		
	F	−0.246			0.557			3.364		
CH_4[d]	C	−0.08			0.93			4.12		
	H	0.02			0.42			2.92		
N_2[e]	N	0.377			0.93			3.51		
	q[e]	−0.377			0.00			1.00		
Ar	Ar	0.0			1.66			3.76		

[a] $r_{ii}=2r_i$, where r_i is the van der Waals radius of atom i.

[b] See Table I for the charge calculation. α_i and r_{ii} values of A and B states are estimated from the experimental shift of one cluster (see the text).

[c] Geometry from Ref. 36. Charges are calculated with the GAUSSIAN 94 program[34] at MP4/6-311G** level. r_{ii} of the fluorine atom is from Ref. 37.

[d] Geometry and charges from Ref. 38.

[e] Charges added to simulate the N_2 quadrupolar moment.

data for fitting the A state potential energy surface. α_i and r_{ii} of N, C, and O atoms in the NCO A state are adjusted so that the calculated spectroscopic shift of the $\tilde{A} \leftarrow \tilde{X}$ transition of $NCO(N_2)_1$ matches the experimental value of 22.6 cm^{-1}. With these adjusted parameters, the binding energies and geometries of the other clusters in the $\tilde{A}$ state are calculated. Parameters used for calculation and the calculated results are listed in Tables II and III. The calculated spectroscopic shift for $NCO(CF_4)_1$ is quite close to the experimental value. For $NCO(Ar)_1$ and $NCO(CH_4)_1$, the calculations indicate that the binding energies for the A state are very close to those for ground state. These small calculated shifts suggest that the cluster transitions for $\tilde{A} \leftarrow \tilde{X}$ of $NCO(Ar)_1$ and $NCO(CH_4)_1$ may lie under the NCO origin feature.

The geometries of $\tilde{A}$ state clusters obtained by these calculations are again very close to those of the ground state clusters. For $NCO(CF_4)_1$ another minimum energy position is found that places the CF_4 molecule near the $N{=}C$ bond side of NCO, and is roughly 20 cm^{-1} higher in energy. The barrier between these two $\tilde{A}$ state minima is only a few wave numbers. Probably only one structure is present for our experimental conditions.

van der Waals frequency calculations[32] are performed for the two clusters with multiple features for their $\tilde{A} \leftarrow \tilde{X}$ transition bands. For clusters in the $\tilde{A}$ state, the vibrational mode energies are calculated as 7.9, 8.2, 24.4, and 35.3 cm^{-1} for $NCO(N_2)_1$, and 9.3, 18.8, 21.0, 30.8, and 54.6 cm^{-1} for $NCO(CF_4)_1$, respectively. As shown in Fig. 5(a), the three distinguishable features to the blue of the $NCO(CF_4)_1$ $\tilde{A} \leftarrow \tilde{X}$ transition origin are separated by 10.7, 16.5, and 31.8 cm^{-1} from it, respectively. In the case of $NCO(N_2)_1$, the first two features to the blue of its $\tilde{A} \leftarrow \tilde{X}$ transition origin are 23.8 and 32.9 cm^{-1} away from its origin feature, respectively. An apparent agreement between some of the calculated and experimental van der Waals mode energies can be suggested. These results are tabulated in Table IV. Again, this agreement emphasizes the reasonableness of the above analysis procedure.

Band contours are simulated for the $\tilde{B} \leftarrow \tilde{X}$ transition bands of NCO clusters using rotational constants derived from cluster geometry obtained in the above calculations. As can be seen from the rotational constants listed in Table V, all clusters are near symmetric top rotors. Spectroscopic resolution used for the simulations is 0.8 cm^{-1}. Rotational

TABLE III. Binding energy (E_B) and spectroscopic shift (δ) of NCO clusters obtained from potential energy calculations (cm^{-1}).[a]

Solvent		Ar	CH_4	N_2	CF_4
X	E_B	187.7	248.5	230.5	418.4
A	E_B	176.2(188.6)	230.3(250.9)	207.9(227.3)	363.7(419.4)
	$\delta_{\text{calc.}}$	11.5	18.2	22.6	54.7
	δ_{exp}	⋯	⋯	22.6	37.4
B	E_B	142.0(185.9)	184.1(247.0)	168.3(229.1)	308.1(427.4)
	$\delta_{\text{calc.}}$	45.7	64.4	62.2	110.3
	δ_{exp}	45.7	58.5	88.0	21.4

[a] For the B state, the α_i and r_{ii} parameters of NCO are adjusted for $NCO(Ar)_1$ to match the experimental results. For the A state, the α_i and r_{ii} parameters of NCO are adjusted for $NCO(N_2)_1$ to match the experimental results. The E_B values in parentheses are calculated without adjusting α_i and r_{ii} values.

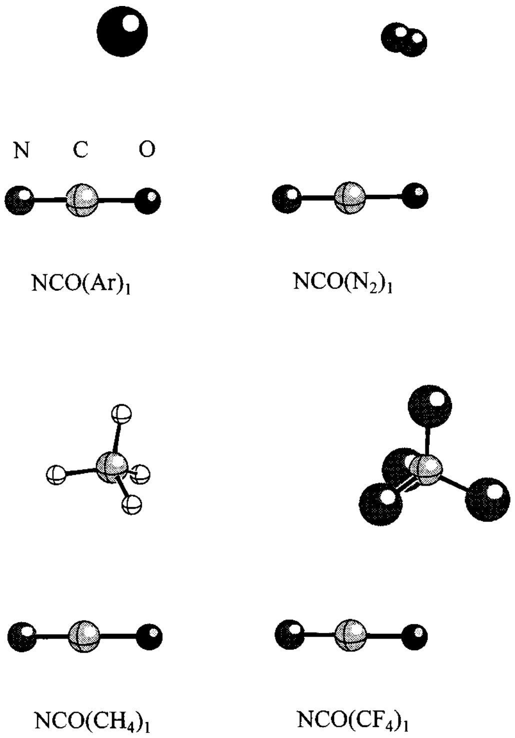

FIG. 6. Ground state geometry of NCO clusters obtained from potential energy calculations. Excited $\tilde{A}$ and $\tilde{B}$ state geometries would look identical on this scale.

TABLE V. Parameters for band shape simulations of the $\tilde{B}\leftarrow\tilde{X}$ transition bands of NCO clusters, obtained from potential energy calculations.

	Rotational constants (10^{-2} cm^{-1})						
	Ground state X			Excited state B			Band composition (%)
Solvent	A''	B''	C''	A'	B'	C'	(A type/B type)[a]
Ar	38.31	6.34	5.44	33.32	6.04	5.11	0/100
N$_2$	31.70	7.89	6.85	35.53	6.84	5.73	28/72
CH$_4$	35.40	11.12	8.60	31.13	10.58	8.02	19/81
CF$_4$	13.38	3.33	3.10	12.94	3.13	2.91	34/66

[a] This designation refers to Hund's classifications for ''band types,'' as explained by G. Herzberg, *Electronic Spectra of Polyatomic Molecules* (van Nostrand, Princeton, 1966).

bands for all clusters are simulated with a mixed band type as indicated in Table V. The mixed band compositions are estimated as follows: since in all the clusters the NCO radical lies in the plane of the a,b rotational axes, and the perturbation of a solvent molecule on the $\tilde{B}\leftarrow\tilde{X}$ electronic transition dipole moment should be small, the transition dipole moment should still be oriented along the NCO radical bond axis, and the ratio of its projections along the a and b axes can be estimated. This ratio actually represents the ratio of $\tilde{A}$ and $\tilde{B}$ band-type components in the rotational band shape. As can be seen from Fig. 3(b), all simulated band shapes agree reasonably well with experimental ones. This shows that the potential energy calculations performed in this work are at least qualitatively correct in predicting cluster geometry.

This approach is not applicable to the $\tilde{A}\leftarrow\tilde{X}$ transitions of the NCO radicals, since the electronic transition dipole moment is perpendicular to the NCO radical band axis, and does not have an *a priori* fixed orientation within the a, b, and c axes system. Therefore we can not simply estimate the rotational band composition for the $\tilde{A}\leftarrow\tilde{X}$ cluster transitions.

To estimate the contribution from the Coulomb interaction, potential energy calculations are performed for all the clusters without adjustment in α_i and r_{ii} values but including both ground and excited state atomic charges. The data presented in Table III (in parentheses), show that the excited state binding energies thus calculated are all within a few wave numbers of the ground state ones. This clearly demonstrates that the van der Waals interaction contributes most to the changes in binding energies of the clusters at different electronic states.

TABLE IV. Calculated and observed van der Waals mode energies (cm^{-1}) for the 1:1 clusters in the A electronic state.

NCO(N$_2$)$_1$		NCO(CF$_4$)$_1$	
Calc.	Exp.	Calc.	Exp.
35.3	32.9	54.6	⋯
24.4	23.8	30.8	31.8
8.2	⋯	21.0	⋯
7.9	⋯	18.8	16.5
	⋯	9.3	10.7

2. 1:*n* *clusters*

With relatively higher backing pressures and higher solvent molecule concentration in the backing gas, we have observed fluorescence signals that we believe belong to NCO clusters containing multiple solvent molecules for all the four solvents. Such spectra are observed for both $\tilde{A}$ and $\tilde{B}$ electronic states. These signals are pressure and solvent concentration dependent. They are all broad, and have fluorescence decay lifetimes and wavelengths similar to the 1:1 NCO clusters with the four solvents.

The spectroscopic shifts of these larger clusters are somewhat surprising. As is shown in Fig. 7, the transitions for these clusters can have either red or blue shifts with respect to the NCO transitions.

The $\tilde{A}\leftarrow\tilde{X}$ transition bands of NCO(N$_2$)$_n$ and NCO(CF$_4$)$_n$ are slightly to the blue of the 1:1 cluster bands. At high pressure and with high solvent concentration, the 1:1 cluster bands of NCO with CF$_4$ are submerged in their 1:n cluster bands, as is shown in Fig. 7(b).

Although we have not observed the $\tilde{A}\leftarrow\tilde{X}$ transition bands of NCO(Ar)$_1$ and NCO(CH$_4$)$_1$ to the blue of the NCO AX origin, with 500 psi pressure and with a high concentration of solvent, we do observe weak broad features to the red of the NCO $\tilde{A}\leftarrow\tilde{X}$ transition origin under these conditions, as shown in Fig. 7(a). These weak broadbands are probably the 1:n cluster bands of NCO with Ar and CH$_4$.

The $\tilde{B}\leftarrow\tilde{X}$ transitions of all 1:n clusters show a red shift in their spectra. Figure 7(c) shows $\tilde{B}\leftarrow\tilde{X}$ transition bands of NCO clusters with Ar and CF$_4$. In the $\tilde{B}(000)\leftarrow\tilde{X}(000)$

transition region of NCO, in addition to the strong $NCO(Ar)_1$ and $NCO(CF_4)_1$ peaks observed at 31 814.2 and 31 789.9 cm^{-1}, respectively (marked with an asterisk in Fig. 7), broad features appear to the red of the NCO origin peaks. These red shifted broad peaks belong apparently to $NCO(Ar)_n$ and $NCO(CF_4)_n$. Note that in Fig. 7(c), the sharp features of the NCO radical show low intensities due to the insertion of an L42 filter (transmission of >410 nm) in front of the photo tube detecting fluorescence. The very low-intensity ratio of the 31 768.5 cm^{-1} feature to the 31 746.0 cm^{-1} is due to both the insertion of the L42 filter and a 50 ns delay in fluorescence signal acquisition for the purpose of avoiding scattered light interference.

Note that even in the absence of a $\tilde{B}(100)\leftarrow\tilde{X}(000)$ transition observed for the 1:1 clusters, features to the red of $\tilde{B}(100)\leftarrow\tilde{X}(000)$ for NCO are observed with similar intensity and broadness as those observed to the red of the NCO $\tilde{B}(100)\leftarrow\tilde{X}(000)$ transition [see Fig. 7(c)]. This will be further discussed in the next section.

We do not have a good explanation for the diverse behavior of the spectroscopic shifts for $NCO(X)_n$ $(n>1)$ clusters. Previous calculations[32] for $CH_3O(X)_n$ $(n>1)$ clusters gave a semiquantitative prediction of the spectroscopic shifts. The calculated results for $NCO(X)_n$ $(n>1)$ clusters do not match the experimental results: contrary to experimental results, calculations predict blue shifts for all the cluster transitions of $NCO(X)_n$ $(n>1)$.

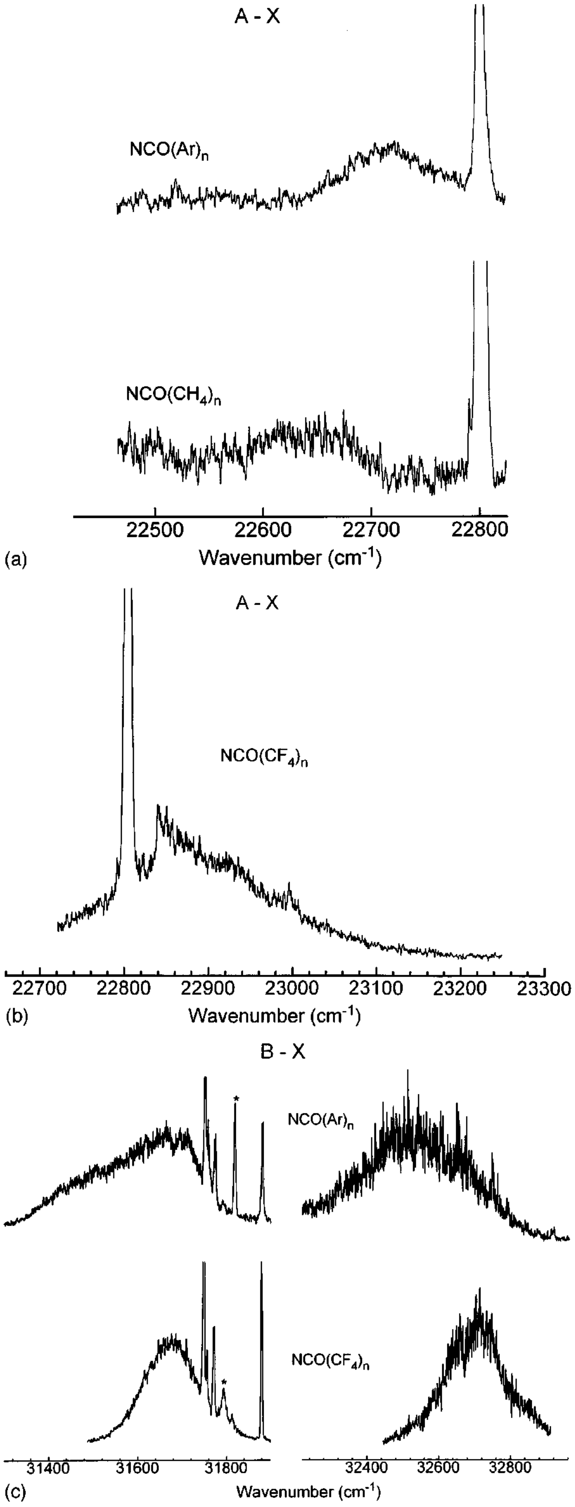

FIG. 7. (a) FE spectra of the $\tilde{A}\leftarrow\tilde{X}$ transition of $NCO(Ar)_n$ and $NCO(CH_4)_n$. The broad features to the red of the NCO $\tilde{A}\,^2\Sigma^+\leftarrow\tilde{X}\,^2\Pi_{3/2}$ at 22 800 cm^{-1} belong to these clusters. Pure argon and 10% CH_4 in helium are used as backing gases for $NCO(Ar)_n$ and $NCO(CH_4)_n$, respectively. (b) FE spectrum of the $\tilde{A}\leftarrow\tilde{X}$ transition of $NCO(CF_4)_n$. The broad feature commencing to the red of the NCO $\tilde{A}\,^2\Sigma^+\leftarrow\tilde{X}\,^2\Pi_{3/2}$ transition at 22 800 cm^{-1} belongs to these clusters. 0.5% CF_4 in helium is used as backing gas. (c) FE spectra of the $\tilde{B}\leftarrow\tilde{X}$ transition of 1:n NCO clusters. The broad features belong to these clusters. Pure argon and 1% CF_4 in helium are used as backing gases for $NCO(Ar)_n$ and $NCO(CF_4)_n$ detection, respectively. Features of 1:1 clusters are labeled with asterisks.

C. Decay pathways

Previous studies,[19(a),21] as well as our observations, have demonstrated that the lifetime of the NCO radical in the $\tilde{B}$ state vibronic levels shortens dramatically with increasing energy. Dissociation products are also detected by Neumark *et al.*[22] As is mentioned in the Introduction, Alexander and Werner[30] proposed that a crossing between the $\tilde{B}$ and $\tilde{A}$ and states of NCO exists, and that another crossing between $\tilde{A}\,^2\Sigma^+$ and the repulsive $^4\Sigma^-$ state also can be suggested. Both crossings are within a few hundred wave numbers of the $\tilde{B}\,^2\Pi(000)$ level. The eventual crossing of the NCO radical from the $\tilde{A}$ or $\tilde{B}$ state potential surface to the dissociative potential surface $^4\Sigma^+$ is the cause of the unusual lifetime shortening and the formation of dissociation products in the $\tilde{B}$ vibronic levels of the NCO radical near and above the crossing intersections.

All $\tilde{B}$ state clusters fluoresce only to the red of 390 nm (25 641 cm^{-1}), and have a fluorescence decay lifetime in the range of 250–320 ns compared to a lifetime of 90 ns for the $\tilde{B}$ state origin of the bare radical. This strongly suggests that the $\tilde{B}$ state NCO clusters have a different decay pathway than does the $\tilde{B}$ state of the bare NCO radical itself.

In the case of 1:1 NCO clusters at the $\tilde{B}(000)$ level, instead of observing a shortened lifetime through direct radiative and indirect dissociative decay, as in the case for the bare NCO radical, we actually observe a fluorescence wavelength range and decay lifetimes that match those of $\tilde{A}$ state vibronic levels lower in energy than 25 640 cm^{-1}. A pos-

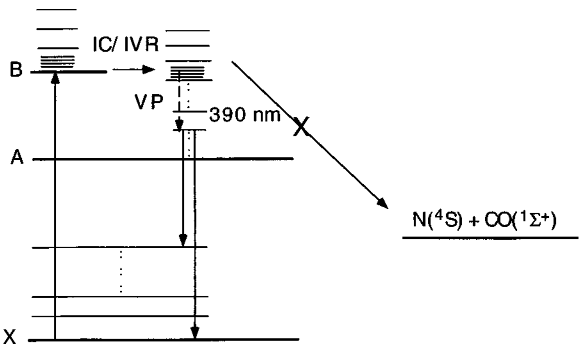

FIG. 8. A schematic diagram of the decay pathway of $\tilde{B}$ state NCO clusters. Clusters at B vibronic levels first internal convert to nearby $\tilde{A}$ vibronic levels (plus van der Waals modes as required for energy conservation), and then undergo IVR/VP (intracluster vibrational redistribution/vibrational predissociation). NCO fragments are formed at $\tilde{A}$ state vibronic levels lower than *ca.* 25 640 cm^{-1} in energy, and subsequently fluoresce.

sible decay pathway for these $\tilde{B}$ state NCO clusters is depicted in Fig. 8. After a NCO cluster is excited to a $\tilde{B}$ vibronic level, it first internally converts to an $\tilde{A}$ vibronic level (IC/IVR), then undergoes further IVR to populate (more) van der Waals modes and lower $\tilde{A}$ state vibronic levels, and finally undergoes vibrational predissociation (VP), generating a translationally hot solvent molecule and a bare NCO $\tilde{A}$ state radical. The NCO radical is in an A vibronic state with an energy lower than 25 640 cm^{-1} [the highest possible level is an $\tilde{A}$ (040) level]. The $\tilde{A}$ vibronic state NCO fragment then fluoresces with a decay lifetime longer than 250 ns. This fluorescence is actually what we detected for the $\tilde{B}\leftarrow\tilde{X}$ transition of NCO clusters. The IVR/VP rate is apparently fast and prevents NCO dissociative decay through crossing to the $^4\Sigma^-$ state.

The energy difference between the $\tilde{B}(000)$ state cluster and the 25 640 cm^{-1} level is more than 6100 cm^{-1}. In the decay process, this energy is distributed into transitional and rotational energy for both the NCO fragment and the solvent molecule.

As is shown in Fig. 3(a) the NCO feature at 31 746.0 cm^{-1} has an intensity not much lower than that of the $\tilde{B}\ ^2\Pi_{3/2}(000)$ dominant band at 31 768.5 cm^{-1}; however, only one 1:1 cluster band is observed for each NCO cluster. A possible explanation is that the lifetime of the cluster in the $\tilde{A}$ state dominant vibronic level corresponding to the 31 746 cm^{-1} feature is so short that the cluster at this level decays through IVR/VP on a subpicosecond time scale. The $\tilde{A}$ vibronic level cluster states at this energy may thus be lifetime broadened and may not be observed. For the cluster at the $\tilde{B}\ ^2\Pi(000)$ dominant level, a long lifetime arises due to the slower IC/IVR process. Once the cluster crosses to an $\tilde{A}$ vibronic level, it experiences the same IVR/VP and subsequent fragment fluorescence. Thus, the increased lifetime of the $\tilde{B}$ state cluster enables us to detect a reasonably well-defined spectroscopic feature for the cluster at *ca.* 31 800 cm^{-1}.

In Sec. III B, we mention that clusters of NCO(X)_n ($n>1$) have decay lifetimes and wavelength ranges similar to those of the 1:1 clusters. These larger clusters at the $\tilde{B}(000)$ state probably experience a similar decay scheme by first crossing to nearly degenerate $\tilde{A}$ vibronic levels, and then decaying through IVR/VP to generate $\tilde{A}$ state bare NCO radicals.

For a 1:1 cluster at the $\tilde{B}(100)$ level [$\tilde{B}(000)+1000\ \text{cm}^{-1}$], the cluster can decay (VP) to NCO $\tilde{B}(000)$ and a ground state solvent molecule. Since the absorption is broad and weak, no fluorescence excitation spectra are observed, as is also the case for the $\tilde{A}$ state cluster level at 31 746.0 cm^{-1}. Larger clusters at the $\tilde{B}(100)$ level do not totally fragment at this energy due to slower VP and thus are weakly observed through the $\tilde{B}(000)\rightarrow\tilde{A}(lmn)\rightarrow$IVR/VP pathway.

IV. SUMMARY AND CONCLUSIONS

Using LIF techniques, we have investigated NCO and its clusters with the nonpolar solvents Ar, N_2, CH_4, and CF_4 for transitions from the $\tilde{X}\ ^2\Pi_{3/2}(000)$ level to vibronic levels of both the $\tilde{A}$ and $\tilde{B}$ electronic states. Transitions for the $\tilde{B}\ ^2\Pi_{3/2}(100)\leftarrow\tilde{X}\ ^2\Pi_{3/2}(000)$ and $\tilde{A}\ ^2\Sigma^+(100)\leftarrow\tilde{X}\ ^2\Pi_{3/2}(000)$ region of the bare radicals agree with previous work. We believe that the three bands in the region of $\tilde{B}\ ^2\Pi_{3/2}(000)\leftarrow\tilde{X}\ ^2\Pi_{3/2}(000)$ transition arise from the mixing of $\tilde{B}\ ^2\Pi_{3/2}(000)$ and $\tilde{A}$ state vibronic levels. The two bands with lower intensity and longer decay lifetime are more $\tilde{A}$ dominant, while the feature at 31 768.5 cm^{-1} with the highest intensity and the shortest lifetime is more likely $\tilde{B}^2\Pi_{3/2}(000)$ dominant.

All observed transitions of 1:1 NCO clusters show blue shifts in their spectra; this shift indicates a smaller cluster binding energy in the cluster excited states. Potential energy calculations are performed to estimate binding energies as well as to find cluster geometry in different electronic states. All four solvents tend to cluster with NCO at the side of the C=O bond. The change of cluster binding energy for different electronic states is mainly caused by changes in the α_i and r_{ii} potential parameters of the atoms in NCO; in other words, by changes in the van der Waals dispersion interaction. van der Waals mode calculations for 1:1 clusters are in reasonable agreement with the observed cluster vibrational modes of the A state.

While NCO radicals at low $\tilde{B}$ state vibronic levels decay through radiative and dissociative (via crossing to a $^4\Sigma^+$ surface) pathways, the observed $\tilde{B}$ state NCO clusters seem to decay through first crossing to $\tilde{A}$ vibronic levels, followed by a very fast IVR/VP process. Subsequent NCO fragments are formed at $\tilde{A}$ vibronic levels lower in energy than 25 640 cm^{-1} and fluoresce.

Note added in proof. As an additional confirmation that the vibronic bands observed ca. 31 750 cm^{-1} [Figs. 3(a) and 4] arise from the mixing of $\tilde{B}\ ^2\Pi_{3/2}(000)$ and $\tilde{A}$ vibronic levels, the spectrum of NCO taken in the $\tilde{B}\ ^2\Pi_{3/2}(000)\leftarrow\tilde{X}\ ^2\Pi_{3/2}(000)$ region at ca. 20 K matches well the rotational band contours by Professor P. J. Dagdigian.[21(b)] This simulation is based on the Dixon Hamiltonian[13] that includes the appropriate $\tilde{A}$-$\tilde{B}$ state vibronic coupling.

ACKNOWLEDGMENTS

This work is supported in part by grants from the USNSF and USARO. One of us (JAF) thanks the Basque Government for a postdoctoral fellowship. We wish to thank Professor P. J. Dagdigian and Professor M. H. Alexander for providing us an unpublished manuscript of the theoretical work by M. H. Alexander and H. J. Werner. We additionally thank Professor P. J. Dagdigian for helpful discussions and for providing us with his simulation results of the rotational band contours for the NCO $\tilde{B}\,^2\Pi_{3/2}(000)\leftarrow\tilde{X}\,^2\Pi_{3/2}(000)$ region.

[1] (a) B. S. Haynes, D. Iverach, and N. Y. Kirov, in *15th Symposium (International) on Combustion* (The Combustion Institute, Pittsburgh, 1974), p. 1103; (b) B. S. Haynes, Combust. Flame **28**, 113 (1977).

[2] C. P. Fenimore, Combust. Flame **26**, 249 (1976).

[3] C. Morely, Combust. Flame **27**, 189 (1976).

[4] J. A. Miller, M. C. Branch, W. J. Mclean, D. W. Chandler, M. D. Smooke, and R. J. Kee, in *20th Symposium (International) on Combustion* (The Combustion Institute, Pittsburgh, 1984), p. 673.

[5] M. H. Alexander, P. J. Dagdigian, M. E. Jacox, C. E. Kolb, C. F. Melius, H. Rabitz, M. D. Smooke, and W. Tsang, Prog. Energy Combust. Sci. **17**, 263 (1991).

[6] J. N. Mulvihill, and L. F. Philips, in Ref. 1, p. 113.

[7] (a) W. R. Anderson, T. A. Vanderhoff, A. J. Kotlar, M. A. Dewilde, and R. A. Beyer, J. Chem. Phys. **77**, 1677 (1982); (b) K. N. Wong, W. R. Anderson, A. J. Kotler, and J. A. Vanderhoff, *ibid.* **81**, 2970 (1984).

[8] D. G. Sauder, D. Patel-Misra, and P. J. Dagdigian, J. Chem. Phys. **95**, 1696 (1991).

[9] B. Ruscic and J. Berkowitz, J. Chem. Phys. **100**, 4498 (1994).

[10] C. J. Astbury, G. Hancock, and K. G. Mckendrick, J. Chem. Soc. Faraday Trans. **89**, 405 (1993).

[11] (a) J. A. Fernandez, Ph.D. thesis, Universidad der Pais Vasco, 1995; (b) J. A. Fernandez, I. Merrelas, D. Husian, M. N. Sanchez Rayo, and F. Castano, Chem. Phys. Lett. **267**, 301 (1997); (c) J. A. Fernandez, P. Payuclo, D. Husain, M. N. Sanchez Rayo, and F. Castano, J. Chem. Phys. **106**, 7090 (1997).

[12] (a) R. N. Dixon, Philos. Trans. R. Soc. London, Ser. A **252**, 165 (1960); (b) Can. J. Phys. **38**, 10 (1960).

[13] R. N. Dixon, M. J. Trenouth, and C. M. Western, Mol. Phys. **60**, 779 (1987).

[14] D. E. Milligan, and M. E. Jacox, J. Chem. Phys. **47**, 5157 (1967).

[15] V. E. Bondybey and J. H. English, J. Chem. Phys. **67**, 2868 (1977).

[16] H. Reisler, M. Mangir, and C. Wittig, Chem. Phys. **47**, 49 (1980).

[17] G. Hancock and G. W. Ketley, J. Chem. Soc. Faraday Trans. **278**, 1283 (1982).

[18] T. R. Charlton, T. Okamura, and B. A. Thrush, Chem. Phys. Lett. **89**, 98 (1982).

[19] (a) B. J. Sullivan, G. P. Smith, and D. R. Crosley, Chem. Phys. Lett. **96**, 307 (1983); (b) R. A. Copeland and D. R. Crosley, Can. J. Phys. **62**, 1448 (1984).

[20] (a) D. Patel-Misra, D. G. Sauder, and P. J. Dagdigain, J. Chem. Phys. **93**, 5448 (1990), and reference therein; (b) D. Patel-Misra, D. G. Sauder, P. J. Dagdigain, and D. R. Crosley, *ibid.* **95**, 2222 (1991).

[21] (a) S. A. Wright and P. J. Dagdigian, J. Chem. Phys. **104**, 8279 (1996); (b) P. J. Dagdigian (private communication).

[22] D. R. Cyr, R. E. Continetti, R. B. Metz, D. L. Osborn, and D. M. Neumark, J. Chem. Phys. **97**, 4937 (1992).

[23] (a) P. S. H. Bolman, J. M. Brown, A. Carrington, I. Kop, and D. A. Ramsay, Proc. R. Soc. London, Ser. A **343**, 17 (1975); (b) P. Misra, C. W. Mathews, and D. A. Ramsay, J. Mol. Spectrosc. **130**, 419 (1988).

[24] D. R. Woodward, D. A. Flether, and J. M. Brown, Mol. Phys. **62**, 517 (1987).

[25] R. Bruggemann, M. Petri, H. Fischer, D. Mauer, D. Reinert, and W. Urban, Appl. Phys. B: **48**, 105 (1990).

[26] (a) C. E. Barnes, J. M. Brown, A. D. fackerell, and T. J. Sears, J. Mol. Spectrosc. **92**, 485 (1982); (b) J. Werner, W. Seebass, M. Koch, R. F. Curl, W. Urban, and J. M. Brown, Mol. Phys. **56**, 453 (1985).

[27] P. B. Davies and I. H. Davis, Mol. Phys. **69**, 175 (1990).

[28] (a) K. Kawaguchi, S. Saito, and E. Hirota, Mol. Phys. **49**, 663 (1983); (b) **55**, 341 (1985).

[29] (a) F. J. Northrup, M. Wu, and T. J. Sears, J. Chem. Phys. **96**, 7218 (1992); (b) M. Wu, F. J. Northrup, and T. J. Sears, *ibid.* **97**, 4583 (1992).

[30] M. H. Alexander and H. J. Werner (private communication).

[31] S. Sun and E. R. Bernstein, J. Chem. Phys. **103**, 4447 (1995).

[32] J. A. Fernandez, J. Yao, and E. R. Bernstein, J. Chem. Phys. (to be published).

[33] (a) R. A. Scott and H. A. Scheraga, J. Chem. Phys. **45**, 2091 (1966); (b) F. A. Momany, L. M. Carruthers, R. F. McGuire, and H. A. Scheraga, *ibid.* **78**, 1595 (1974); (c) G. Nemethy, M. S. Pottle, and H. A. Scheraga, *ibid.* **87**, 1883 (1988).

[34] M. J. Frisch, G. W. Trucks, H. B. Schlegel, P. M. W. Gill, B. G. Johnson, M. A. Robb, J. R. Cheeseman, T. A. Keith, G. A. Petersson, J. A. Montgomery, K. Raghavachari, M. A. Al-Laham, V. G. Zakrzewski, J. V. Ortiz, J. B. Foresman, J. Cioslowski, B. B. Stefanov, A. Nanayakkara, M. Challancombe, C. Y. Peng, P. Y. Ayala, W. Chen, M. W. Wong, J. L. Andres, E. S. Replogle, R. Gomperts, R. L. Martin, D. J. Fox, J. S. Binkley, D. J. Defrees, J. Baker, J. P. Stewart, M. Head-Gordon, C. Gonzalez, and J. A. Pople, GAUSSIAN 94, Gaussian Inc., Pittsburgh, PA, 1995.

[35] (a) M. T. Martinez (private communication); (b) R. Pereira, I. Alava, F. Castano, and M. T. Martinez, J. Chem. Soc. Faraday Trans. **90**, 2443 (1994); (c) R. Pereira, T. Calvo, F. Castano, and M. T. Martinez, Chem. Phys. **201**, 433 (1995).

[36] *Handbook of Chemistry and Physics*, 76th (1995–1996) ed. (CRC Press, Boca Raton, 1995).

[37] A. K. Rappe, C. J. Casewit, K. S. Colwell, W. A. Goddard, III, and W. M. Skiff, J. Am. Chem. Soc. **114**, 10 026 (1992).

[38] (a) A. D. Buckingham, and P. W. Fowler, J. Chem. Phys. **79**, 6426 (1993); (b) G. J. B. Hurst, P. W. Fowler, A. J. Stone, and A. D. Buckingham, Int. J. Quantum Chem. **29**, 1223 (1986).